12^{th} International Conference on Fracture Mechanics of Concrete and Concrete Structures
FraMCoS-12
B.L.A. Pichler, Ch. Hellmich, P. Preinstorfer (Eds)

https://doi.org/10.21012/FC12.1159
MS05-1:2

MODELING CONCRETE AT HIGH-LOADING RATES: INSIGHTS BY THE MATERIAL POINT METHOD

O. ANDRES OROPEZA-NAVARRO*, JAKOB PLATEN*, AHMAD CHIHADEH* AND MICHAEL KALISKE*†

* Technische Universität Dresden, Institute for Structural Analysis
01062 Dresden, Germany
† corresponding author: michael.kaliske@tu-dresden.de

Key words: material point method, microplane damage model, nonlocal formulation

Abstract. The modeling and simulation of concrete structures at high-loading rates is an important topic in computational mechanics, as it can be relevant to improving the safety and durability of structures. High-loading rates on concrete structures may occur during explosions, or impacts. Mesh-based methods often encounter difficulties in these scenarios due to potentially high mesh distortion in these regions. However, the Material Point Method (MPM) is well-suited for modeling situations involving large deformations, as it uses a continuously reset computational mesh.

Additionally, modeling concrete that exhibits strain softening behavior requires regularization methods to solve strain localization and mesh dependency issues. One of the leading methods is implicit gradient enhancement, which is based on a nonlocal formulation, where an additional degree of freedom is introduced to be solved in the linearized system of equations.

In this work, the MPM is used with a regularized microplane damage material model at finite deformation to describe concrete behavior at high loading rates.

1 Introduction

Concrete structures play a dominating role in modern constructions due to their durability, versatility, and cost-effectiveness, making them widely used in buildings, bridges, dams, and protective facilities. However, these structures could be subjected to extreme events such as impacts, blasts, or accidental collisions, which impose extreme and dynamic loading conditions. Under such scenarios, concrete exhibits complex nonlinear behavior, including cracking, crushing, and fragmentation. Modeling these phenomena, using mesh-based methods, such as the Finite Element Method (FEM), often suffers from local mesh distortion at the impacted face. Moreover, the Material Point Method (MPM), introduced by SULSKY [1], can overcome mesh distortion at a reasonable computational cost. Numerous studies related to MPM use explicit time integration schemes. In contrast, just a reduced number are based on implicit time integration schemes [2, 3, 4], among others, which benefit from larger time steps and more stable numerical solutions.

Moreover, concrete exhibits a complex material response due to the heterogeneity of its constituents. Initially, concrete yields an elastic isotropic response, but during loading, the formation of microcracks induces anisotropy in its behavior. Over time, the evolution of these microcracks leads to the failure of the structure. One common approach to represent concrete is the microplane model, first introduced by BAẐANT and OH [5]. This model incorporates damage and plasticity [6] and has been generalized to finite strains [7]. An efficient regularized nonlocal microplane model is presented in [8, 9] for FEM, and later introduced into MPM [10]. This contribution utilizes a regularized microplane damage material description in MPM with an implicit time discretization scheme. It is based on [10], including the inertia effects to describe concrete behavior at high loading rates.

2 Material Point Method

The Material Point Method (MPM) is a hybrid numerical technique combining particle and grid-based methods for solving problems in computational mechanics. In MPM, the domain is represented by a set of particles, known as material points, that carry all the data of the body and move through a fixed background grid where the computational calculations are performed. Figure 1 illustrates the computational process in MPM for a single step.

First, the data stored in the material point is projected to the background grid by

$$\square_v = \sum_{p=1}^{np} S_{vp} \square_p, \tag{1}$$

where $\square$ are the corresponding variables. These include external forces $\boldsymbol{f}$, acceleration $\ddot{\boldsymbol{u}}$, velocity $\dot{\boldsymbol{u}}$, and mass m. Subscript v and p denote the variables at nodes and at material points, respectively. S_{vp} are the selected projection functions, and np is the total number of material points that influence the grid node. In the second step, the governing differential equations are evaluated in the background grid, and the system is solved for the unknown displacements $\boldsymbol{u}_v$. The third step involves projecting the resulting data back to the material points, updating their spatial position. Finally, the grid resets to its original undeformed configuration, retaining no information of the body. Consequently, the material points can be located in a different subset of the background grid in each step.

Cell-crossing noise is a well-known problem that affects MPM. This effect arises when material points move between grid cells if standard linear FEM shape functions are used as projection functions, which are C^0-continuous. This causes abrupt changes in the gradient of the shape function, resulting in inaccurate stress values. Different strategies have been developed to mitigate this problem. Some of them use a domain-based projection function such as the generalized interpolation material point method (GIMP) [11], the dual domain material point method (DDMP) [12], or convected particle domain interpolation (CPDI) [13, 14]. Another strategy is based on the employment of B-spline shape functions [15]. In this contribution, the CPDI technique is applied.

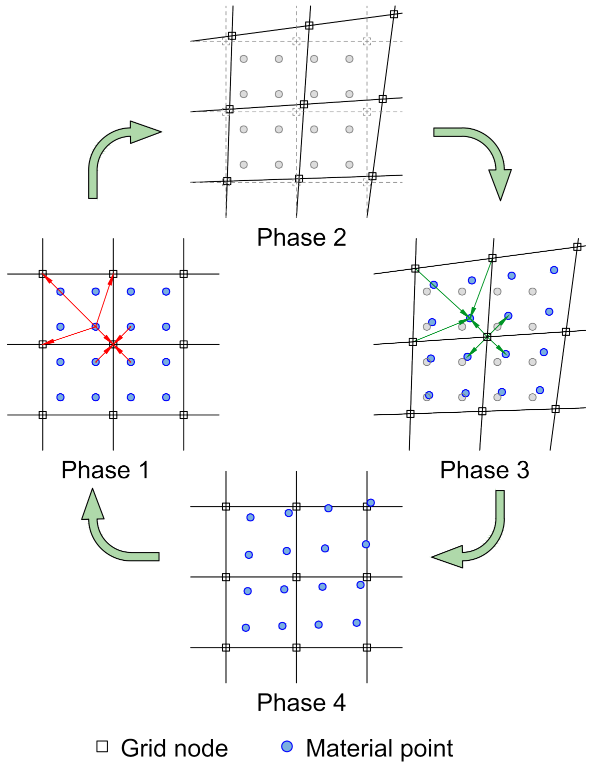

Figure 1: Computational process in MPM.

3 Implicit gradient-enhanced microplane model

In this section, the strain energy density function is defined within the microplane model. The model is regularized by the implicit gradient enhancement at finite strains and implemented into the material point method. Therefore, the concepts from [9, 10, 16, 17], are briefly summarized.

3.1 Nonlocal MPM formulation

The problem is governed by two partial differential equations, which are the balance of linear momentum

$$\nabla \cdot \boldsymbol{\sigma} + \boldsymbol{b} = \rho \ddot{\boldsymbol{u}}, \tag{2}$$

and the modified HELMHOLTZ equation

$$\bar{\eta} - \eta - c\nabla^2 \bar{\eta} = 0. \tag{3}$$

Moreover, Equation (3) can be solved by including the homogeneous NEUMANN boundary condition

$$\nabla \bar{\eta} \cdot \boldsymbol{n}_b = 0. \tag{4}$$

In Equation (2), $\nabla \cdot$ is the divergence operator, $\boldsymbol{\sigma}$ is the CAUCHY stress tensor, $\boldsymbol{b}$ is the mass specific body force vector, ρ is the material density, and $\ddot{\boldsymbol{u}}$ is the acceleration vector. In Equation (3), $\bar{\eta}$ and η are the nonlocal and local equivalent strain of the bulk material, c is the gradient activity parameter, and ∇^2 is the LAPLACE operator. In Equation (4), $\boldsymbol{n}_b$ denotes the unit normal vector to the external boundary, and ∇ is the gradient operator.

Using the test functions $\delta \boldsymbol{u}$ and $\delta \bar{\eta}$, the weak forms of Equations (2) and (3) read

$$\int_{\mathcal{B}} \delta \boldsymbol{u} \cdot \nabla \cdot \boldsymbol{\sigma} \; dv + \int_{\mathcal{B}} \delta \boldsymbol{u} \cdot \boldsymbol{b} \; dv = \int_{\mathcal{B}} \delta \boldsymbol{u} \cdot \rho \ddot{\boldsymbol{u}} \; dv, \tag{5}$$

and

$$\int_{\mathcal{B}} \delta \bar{\eta} \, \bar{\eta} \; dv + \int_{\mathcal{B}} \nabla \delta \bar{\eta} \, c \, \nabla \bar{\eta} \; dv = \int_{\mathcal{B}} \delta \bar{\eta} \, \eta \; dv, \tag{6}$$

respectively.

Introducing the material point discretization defines the displacements at the material points

$$\boldsymbol{u}_p = S_{vp} \boldsymbol{u}_v, \quad \delta \boldsymbol{u}_p = S_{vp} \delta \boldsymbol{u}_v, \tag{7}$$

and the nonlocal variable

$$\overline{\eta}_p = \overline{S}_{vp} \overline{\eta}_v, \quad \delta \overline{\eta}_p = \overline{S}_{vp} \delta \overline{\eta}_v, \tag{8}$$

where $\boldsymbol{u}_p$ and $\boldsymbol{u}_v$ represent the displacements at the material point and at the grid nodes, respectively. $\overline{\eta}_p$ and $\overline{\eta}_v$ denote the nonlocal equivalent strain at the material point and at the grid nodes. In general, it is possible to utilize different projection functions for the displacement field S_{vp} and the nonlocal field $\overline{S}_{vp}$. However, the contribution at hand uses the same projection functions for both fields.

3.2 Nonlocal damage microplane model

The microplane theory provides a simple and straightforward approach to model induced anisotropy. The strategy in the microplane approach is to couple a geometric reference as the basis for the constitutive description at the material point under investigation. It is based on a projection of the deformation tensor onto vectors on randomly oriented planes. In those planes, the constitutive law of the material between the projected strain and stress vectors are applied. The stress tensor is then assembled from the contributions of every plane. The strain energy density function ψ^{mac} can be expressed in terms of microplane quantities as

$$\psi^{mac} = \frac{3}{4\pi} \int_{\Omega} \psi^{mic} dV, \tag{9}$$

considering ψ^{mic} is the strain energy density function on each microplane. In the contribution at hand, the strain energy density function, based on the damage formulation, is taken from [9] and reads

$$\psi^{mic} = (1 - d^{mic}) \left(\frac{1}{2} K^{mic} E_V^2 + G^{mic} \boldsymbol{E}_D \cdot \boldsymbol{E}_D \right). \tag{10}$$

In Equation (10), the bulk modulus K^{mic} and the shear modulus G^{mic} are material parameters that remain constant in all microplanes. E_V and $\boldsymbol{E}_D$ are the volumetric and deviatoric strains projected from the GREEN-LAGRANGE strain tensor onto the microplanes. d^{mic} represents the damage variable in the microplane that reads

$$d^{mic} = 1 - \frac{\gamma_0}{\gamma^{mic}} \left(1 - \alpha + \alpha \exp \beta(\gamma_0 - \gamma^{mic})\right), \tag{11}$$

which is a function of the maximum material degradation parameter α, the softening parameter β, the damage threshold γ_0 and the history variable γ^{mic} on each microplane that drives the evolution of the damage variable, defined as

$$\gamma^{mic}(t) = max(\gamma_0, \overline{\eta}^{mic}). \tag{12}$$

The evolution of the history variable γ^{mic} depends on the nonlocal equivalent strain at each microplane $\overline{\eta}^{mic}$, which is obtained from the local counterpart η^{mic} affected by the ratio of the nonlocal equivalent strain to the maximum local equivalent strain as

$$\overline{\eta}^{mic} = \frac{\overline{\eta}}{\eta} \eta^{mic}. \tag{13}$$

The value of the local equivalent strain η^{mic} at each microplane is obtained as

$$\eta^{mic} = 3k_1 E_V + \sqrt{(3k_1 E_V)^2 + \frac{3}{2} k_2 \boldsymbol{E}_D \cdot \boldsymbol{E}_D}, \tag{14}$$

where k_1 and k_2 are material constants obtained from POISSON'S ratio ν and the ratio of compressive to tensile strength k_r of the material given by

$$k_1 = \frac{k_r - 1}{2k_r(1 - 2\nu)}, \tag{15}$$

and

$$k_2 = \frac{3}{k_r(1 + \nu)^2}. \tag{16}$$

4 Numerical simulation

Subsequently, a compact tension test of pure concrete is simulated. The experimental data are taken from [18]. The geometry and test setup are presented in Figure 2. The tensile load is applied to the specimen in the lower part of the notch as prescribed displacement. The material model parameters are given in Table 1, where the elastic properties of the material are taken from the experimental test [18], while the rest of the parameters are identified to fit the experimental crack patterns. The specimen is tested with three different displacement rates of 0.035 m/s, 1.4 m/s, and 4.3 m/s. The simulation is divided into 1000 time steps with a time increment of $\Delta t = 1 \times 10^{-6}$ s. The size of an individual grid cell of the background grid is 1.0×1.0 mm^2 with 2×2 material points per element with a total of 155530 material points.

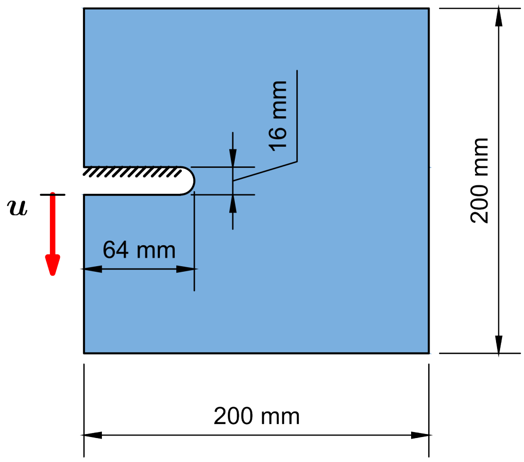

Figure 2: Compact tension test setup.

Material parameters		
K	18,750.00	[MPa]
G	15,254.00	[MPa]
ν	0.18	[-]
γ_0	1.25E-3	[-]
k_r	14	[-]
α	0.98	[-]
β	650.0	[-]
c	1.0	[mm^2]

Table 1: Material parameters for compact tension test.

Figure 3 presents the predicted damage zone obtained by simulations in comparison with experimental crack patterns reported in [18], which present a good correlation for different loading rates. Moreover, it can be seen that at a low loading rate of 0.035 m/s, the damage zone propagates in the same direction as the notch. Moreover, for a loading rate of 1.4 m/s, an inclined damage propagation is observed in Figure 3b. Furthermore, for a loading rate of 4.3 m/s branching of the damage zone is presented in Figure 3c.

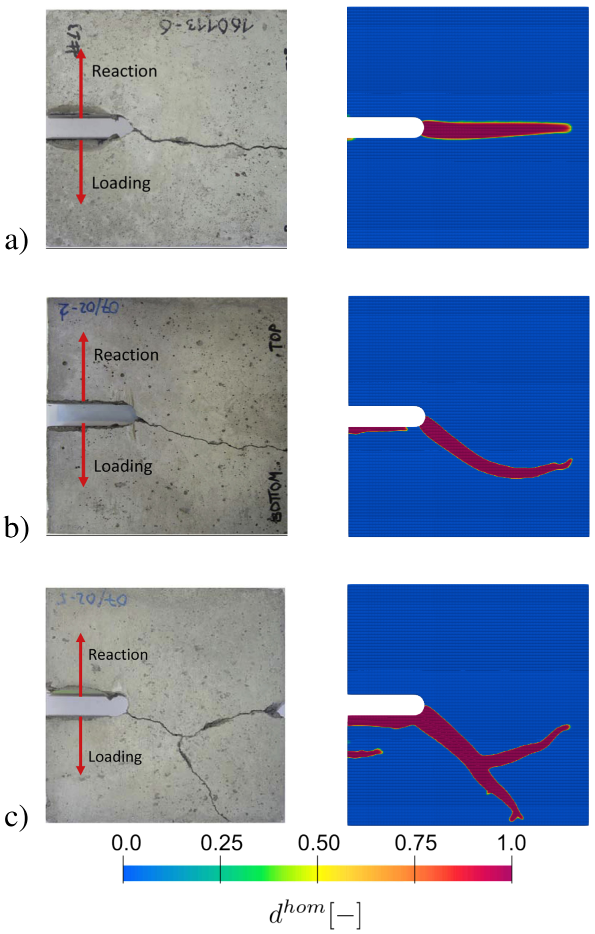

Figure 3: Predicted damage zone and experimental crack patterns [18] for loading rates a) 0.035 m/s, b) 1.4 m/s and c) 4.3 m/s

5 Conclusions

This contribution uses the implicit gradient-enhanced microplane damage material description in the implicit MPM presented in [10], including the inertia effects to address high-loading scenarios in concrete. Through a numerical example, the model demonstrates its capability to capture induced anisotropy and predict damage zones in a reliably and physically consistent manner. Furthermore, strategies to refine the damage zone by evolving the gradient activity parameter c as a function of the nonlocal equivalent strain $\bar{\eta}$ [19, 20], rather than treating it as a constant parameter, will be considered.

6 Acknoledgements

This work is funded by the German Research Foundation (DFG) Grant/Award Number 287321140 within Research Training Group GRK 2250/2 and 2250/3 *"Mineral bonded composites for enhanced structural safety"*, Sub-Project B4, and SFB/TRR 280, Sub-Project A02, Projekt-ID: 417002380 and under Grant KA1163/40 within DFG Priority Programme 2020. This financial support is gratefully acknowledged.

References

[1] D. Sulsky, Z. Chen, and H. Schreyer, 1994, A particle method for history-dependent materials, *Computer Methods in Applied Mechanics and Engineering* **118**: 179–196.

[2] T. Charlton, W. Coombs, and C. Augarde, 2017, iGIMP: An implicit generalised interpolation material point method for large deformations, *Computers and Structures* **190**: 108–125.

[3] A. Chihadeh, W. Coombs, and M. Kaliske, 2023, A coupled implicit MPM-FEM approach for brittle fracture and fragmentation, *Computers and Structures* **288**: 107143.

[4] J. Guilkey and J. Weiss, 2003, Implicit time integration for the material point method: Quantitative and algorithmic comparisons with the finite element method, *International Journal for Numerical Methods in Engineering* **57**: 1323–1338.

[5] Z. P. Bazant and B. H. Oh, 1983, Microplane model for fracture analysis of concrete structures, *Proceeding of Symposium on the Interaction of Non-Nuclear*

Munitions with Structures, U.S. Air Force Academy, Colorado Springs (1983), USA, pp. 49–53.

[6] I. Carol and Z. P. Bazant, 1997, Damage and plasticity in microplane theory, *International Journal of Solids and Structures* **34**: 3807–3835.

[7] Z. P. Bažant, Y. Xiang, and P. C. Prat, 1996, Microplane model for concrete. I: Stress-strain boundaries and finite strain, *Journal of Engineering Mechanics* **122**: 245–254.

[8] B. R. Indriyantho, I. Zreid, R. Fleischhauer, and M. Kaliske, 2020, Modelling of high velocity impact on concrete structures using a rate-dependent plastic-damage microplane approach at finite strains, *Materials* **13**: 5165.

[9] J. Platen, I. Zreid, and M. Kaliske, 2023, A nonlocal microplane approach to model textile reinforced concrete at finite deformations, *International Journal of Solids and Structures* **267**: 112151.

[10] O. A. Oropeza Navarro, A. Chihadeh, J. Platen, and M. Kaliske, 2024, A regularized microplane damage material model in the implicit material point method, *Proceedings in Applied Mathematics and Mechanics* **24**: e202400120.

[11] S. Bardenhagen and E. Kober, 2004, The generalized interpolation material point method, *Computer Modeling in Engineering and Sciences* **5**: 477–496.

[12] D. Z. Zhang, X. Ma, and P. T. Giguere, 2011, Material point method enhanced by modified gradient of shape function, *Journal of Computational Physics* **230**: 6379–6398.

[13] A. Sadeghirad, R. M. Brannon, and J. Burghardt, 2011, A convected particle domain interpolation technique to extend applicability of the material point method for problems involving massive deformations, *International Journal for Numerical Methods in Engineering* **86**: 1435–1456.

[14] A. Sadeghirad, R. M. Brannon, and J. Guilkey, 2013, Second-order convected particle domain interpolation (CPDI2) with enrichment for weak discontinuities at material interfaces, *International Journal for Numerical Methods in Engineering* **95**: 928–952.

[15] M. Steffen, R. M. Kirby, and M. Berzins, 2008, Analysis and reduction of quadrature errors in the material point method (MPM), *International Journal for Numerical Methods in Engineering* **76**: 922–948.

[16] B. J. Dimitrijevic and K. Hackl, 2008, A method for gradient enhancement of continuum damage models, *European Journal of Engineering Mechanics* **28**: 43–52.

[17] I. Zreid and M. Kaliske, 2014, Regularization of microplane damage models using an implicit gradient enhancement, *International Journal of Solids and Structures* **51**: 3480–3489.

[18] J. Ožbolt, J. Bošnjak, and E. Sola, 2013, Dynamic fracture of concrete compact tension specimen: Experimental and numerical study, *International Journal of Solids and Structures* **50**: 4270–4278.

[19] M. Geers, R. De Borst, W. Brekelmans, and R. Peerlings, 1998, Strain-based transient-gradient damage model for failure analyses, *Computer Methods in Applied Mechanics and Engineering* **160**: 133–153.

[20] D. Zhao, B. Yin, S. Tarachandani, and M. Kaliske, 2023, A modified cap plasticity description coupled with a localizing gradient-enhanced approach for concrete failure modeling, *Computational Mechanics* **72**: 787–801.